

Electron tunnel rates in a donor-silicon single electron transistor hybrid

Hans Huebl^{1,2}, Christopher D. Nugroho^{1,3}, Andrea Morello¹,

Christopher C. Escott¹, Mark A. Eriksson⁴, Changyi Yang⁵,

David N. Jamieson⁵, Robert G. Clark¹, and Andrew S. Dzurak^{1*}

¹ *Australian Research Council Centre of Excellence for Quantum Computer Technology,*

Schools of Electrical Engineering and Physics,

The University of New South Wales, Sydney NSW 2052, Australia

² *Walther-Meissner-Institut, Bayerische Akademie*

der Wissenschaften, 85748 Garching, Germany

³ *Department of Physics, University of Illinois at*

Urbana-Champaign, Urbana, Illinois 61801, USA

⁴ *Department of Physics, University of Wisconsin, Madison, Wisconsin 53706, USA*

⁵ *Australian Research Council Centre of Excellence for Quantum Computer Technology,*

School of Physics, The University of Melbourne, Melbourne VIC 3010, Australia

(Dated: May 28, 2022)

Abstract

We investigate a hybrid structure consisting of 20 ± 4 implanted ^{31}P atoms close to a gate-induced silicon single electron transistor (SiSET). In this configuration, the SiSET is extremely sensitive to the charge state of the nearby centers, turning from the off state to the conducting state when the charge configuration is changed. We present a method to measure fast electron tunnel rates between donors and the SiSET island, using a pulsed voltage scheme and low-bandwidth current detection. The experimental findings are quantitatively discussed using a rate equation model, enabling the extraction of the capture and emission rates.

*corresponding author huebl@wmi.badw.de

The readout of a single spin is one of the key elements in spin-based quantum information processing schemes [1, 2]. One may distinguish between single-shot readout, where the projective measurement of a single spin is performed in real time, and “spectroscopic” readout, where the expectation value of the spin state is deduced from a time-averaged quantity (e.g. electrical current, fluorescence emission, ...). Single-shot readout has been demonstrated in GaAs/AlGaAs quantum dots [3, 4], while spectroscopic readout has been obtained in a variety of systems, from quantum dots [5, 6, 7, 8, 9] to NV centers in diamond [10] and dopant atoms in silicon [11]. Carbon and silicon are particularly attractive platforms for solid-state spin-based quantum processors, because they can be isotopically purified to minimize decoherence induced by nuclear spins. However, single-shot readout in these systems has not yet been demonstrated. Recently, an architecture for single-shot readout of a donor spin in silicon was proposed [12], consisting of a single implanted P donor [13] in close proximity to an induced silicon single-electron transistor (SiSET) [14]. The approach employs a readout principle similar to the one successfully demonstrated in GaAs/AlGaAs single quantum dots [3], where the spin state of the electron is deduced from the time-resolved observation of spin-dependent tunneling between the dot and a charge reservoir. However, in the donor-based proposal [12], the bulk charge reservoir is replaced by the island of a SiSET. This configuration is predicted to yield very large charge transfer signals, thereby allowing high-fidelity single-shot spin readout. The timescale of the projective spin measurement is set by the electron tunneling time between donor and SiSET, which must be controlled and understood before attempting spin readout.

In this Letter we demonstrate and investigate the tunneling of electrons in a hybrid device, consisting of approx. 20 ± 4 ^{31}P donors, implanted next to an induced SiSET. We show that the current through the SiSET, I_{SET} , can be switched from zero to the maximum value by transferring an electron from a charge center to the SET island. By applying voltage pulses to a gate near the donors while monitoring I_{SET} , we study the probability for an electron to tunnel between the center and the SiSET. The resulting change in I_{SET} can be understood by considering the donor-SET hybrid system as analogous to a double quantum dot in the parallel configuration [15]. We find that the amplitudes in a pattern of Coulomb peaks depend on the pulse duration and duty cycle, relative to the emission and capture rates for tunneling from or onto the donor. Employing a rate equation model, we are able to extract the electron tunneling rate for a specific charge center. We observe fast tunneling rates of

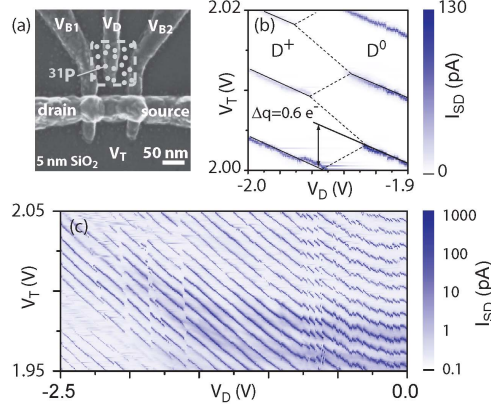


FIG. 1: Scanning electron micrograph of a hybrid device. The P donors are implanted close to an induced SiSET (grey dashed square). The SiSET is formed by two gate controlled (V_{B1}, V_{B2}) tunnel junctions and the overlapping top-gate. Panel (b) displays a close up of the stability diagram near the charge transition of a center with large charge transfer signal $\Delta q \sim 0.6e$. A large gate voltage scan is shown in (c), where various charge transitions from multiple centers are visible.

3000 s^{-1} for the tunnel event to load the center and 1000 s^{-1} for the reverse process, despite the detection bandwidth for the SET (DC) readout being limited to 200 Hz.

Figure 1 (a) shows the device fabricated on a high purity intrinsic silicon wafer ($> 10 \text{ k}\Omega\text{cm}$), with the implantation sites (grey dots) located next to an induced SiSET [14, 16]. In the active device region a high-quality, 5 nm thick silicon oxide is grown by dry thermal oxidation, yielding a very low density of interface traps $\sim 10^{10}/\text{eV}/\text{cm}^2$ near the conduction band edge [17]. Underneath this oxide ohmic contacts are provided ($[P]=5 \times 10^{19} \text{ cm}^{-3}$). In a first electron beam lithography (EBL) step, with subsequent development and evaporation, Ti(15 nm)/Pt(65 nm) alignment markers are formed for a high precision ($< 20 \text{ nm}$) realignment of subsequent layers. A $90 \times 90 \text{ nm}^2$ aperture is opened in the PMMA resist, acting as mask for the ^{31}P donors, which are implanted with an acceleration voltage of 14 keV and at a fluence of $2.5 \times 10^{11} \text{ cm}^{-2}$, resulting in a total of 20 ± 4 ^{31}P donors in this region. After a rapid thermal anneal (1000°C , 5 s) to repair the implantation damage, the Al donor control gate as well as the Al barrier gates of the SiSET are patterned. The surface of these gates is oxidized by an O_2 plasma ash for 4 min at 180°C , resulting in a $\sim 5 \text{ nm}$ thick Al_xO_y insulating layer [18]. An Al top-gate, overlaying the barriers and the source-drain regions, is formed in the last EBL step. This process results in a hybrid quantum system with a few ^{31}P donors in close vicinity to a SiSET. The sample is operated in a dilution refrigerator

at an electron temperature ≈ 200 mK. The source, drain, as well as the SiSET control gates are connected to the room temperature electronics via Cu powder filters with a cut off frequency ~ 1 GHz. The donor control gate is connected via a high-bandwidth line to apply high frequency pulses ($f_{3\text{dB}} \sim 500$ kHz, limited by resistive voltage dividers at room temperature). Its voltage V_D is the sum of a constant component plus a rectangular wave for pulsed voltage spectroscopy. The SiSET DC source-drain current is measured using a current amplifier with 200 Hz bandwidth and a gain of 10^{10}V/A .

The capacitively- and tunnel-coupled donor and the SiSET island effectively form a double quantum dot in parallel configuration [15]. Both series and parallel configurations result in a hexagonal stability diagram, but in the series configuration, transport only occurs at the triple points[19]. In contrast, in the parallel configuration the transport channel is open for any gate voltages for which the electrochemical potential of the SiSET, μ_{SET} , resides in the source-drain bias window. As a result, transport occurs along some of the lines that connect the triple points, which we call transport-lines in the following. Fig. 1 (b) shows these transport-lines in the vicinity of a charge transition, measured with a source-drain bias $V_{\text{SD}} = 50 \mu\text{V}$. The relevant gate space is defined by the top-gate (V_T) of the SiSET and the donor control gate (V_D). When the energy level of the donor is raised with respect to μ_{SET} , at the charge transition point it becomes favorable to remove an electron. This change in the charge configuration (here labeled as $D^0 \rightarrow D^+$ transition) acts back on μ_{SET} and results in a shift of the Coulomb peak lines. The magnitude of the shift in μ_{SET} , relative to the Coulomb peak spacing, is quantified by the charge transfer signal $\Delta q \approx 0.6e$. Since Δq is much larger than the width of the Coulomb peaks, I_{SET} is switched from zero to its maximum value by changing the occupancy of the charge center. The data in Fig. 1 (b) demonstrate the ability to resolve with essentially 100% contrast the charge state of the donor, a critical prerequisite for the spin readout method proposed in Ref. 12.

As shown in Fig 1 (c), the measurement of I_{SET} as a function of V_T and V_D yields a set of Coulomb peaks appearing as tilted lines (due to the cross-capacitance between control gate and SET island) that break at the charge transition points. For $V_D > -0.6$ V the slope of the transport-lines decreases, indicating charge accumulation under the donor control gate. In this regime we find several small charge transitions with $\Delta q < 0.1$, which we interpret as the ionization of shallow charge centers to the Si/SiO₂ interface. At more negative voltages, the pattern clears up, showing well-isolated charge transfers with $0.2 < \Delta q < 0.6$

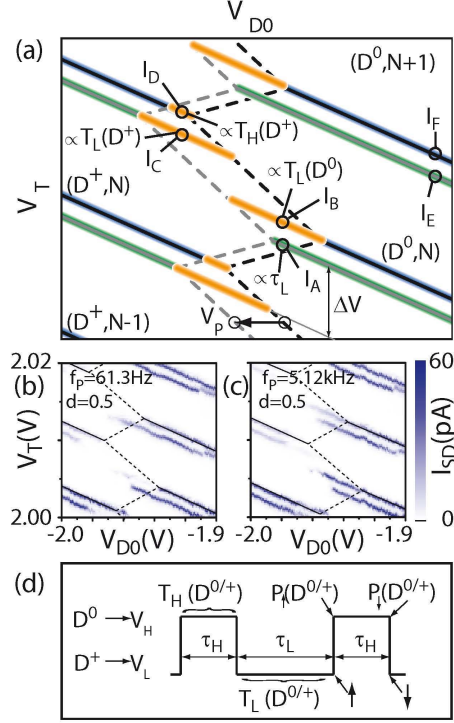


FIG. 2: Charge stability diagram for the pulsed voltage spectroscopy. (a) Sketch of the SiSET conductance as function of the top gate voltage V_T and the dc component of the donor control gate V_{D0} . Drawn as blue (green) lines are the positions of the Coulomb peaks when the added pulse voltage $V_P = V_L = 0$ V ($V_P = V_H$). The dashed lines are guides to the eye to indicate a slice of the hexagonal charge stability diagram characteristic for a double dot system. When the frequency of the square wave f_P for switching between V_L and V_H is much smaller than the tunneling rates Γ_c and Γ_e , no current is observed between the two superimposed stability diagrams (e.g. panel (b), where $f_P = 61.3$ Hz with duty cycle $d = 0.5$), because the charge configuration can follow the equilibrium state. In contrast, when $2\pi f_P \gg \Gamma_c, \Gamma_e$ a non-equilibrium charge configuration can be observed resulting in current along the orange lines. Panel (c) displays I_{SET} for $f_P = 5.12$ kHz, where additional current is visible in this area. Panel (d) shows the schematic for the pulsed voltage imposing a charge transition, indicating the various relevant times for the rate equation model as described in the text.

in agreement with the predicted values for electrons tunneling into the SET island from donors $\sim 30 - 50$ nm away [12], and similar to the values observed in [20] for a charge center near Al- and Si-SETs. This part of the stability diagram is stable and reproducible upon thermal cycling to room temperature.

We stress that the parallel geometrical configuration of our hybrid device impedes direct spectroscopy of the charge center coupled to the SiSET. It is therefore impossible to distinguish a donor from e.g. an interface trap on the basis of its energy levels structure [21]. The number of charge transitions observed for $V_D < -0.6$ V is compatible with the number of donors expected to be found within 30 to 50 nm from the SET island, given the P implant fluence. Furthermore, we note that the charge transitions in this regime typically group in pairs, agreeing in Δq and slope in the V_T - V_D gate space, again compatible with the observations of P donors with two charge transition levels expected [11, 22]. However, the unambiguous identification of the charge center remains a quest for spin readout in combination with magnetic resonance techniques [12]. In this letter, the main focus is on the study of tunnel rates between a SiSET and a charge center, whose precise nature does not affect the results.

We measure the tunnel rates by superimposing on the DC voltage of the donor control gate (V_{D0}) a rectangular wave with frequency f_P , duty cycle d , and amplitude V_P (cf. Fig. 2 (d)). If f_P is slow compared to the (de)charging rate of the center, we record two stability diagrams (blue and green in Fig. 2 (a)), offset by V_P on the horizontal axis when plotted vs. the DC gate voltages V_{D0} and V_T . These arise because any point on the diagram probes the average I_{SET} for the combination of the gate voltages $(V_{D0} + 0 \text{ V}, V_T)$ and $(V_{D0} + V_P, V_T)$. Conversely, if f_P is faster than the electron tunnel rate to/from the charge center, we find $I_{SET} \neq 0$ at gate configurations where transport would be otherwise suppressed, which we call non-equilibrium transport-lines in the following (cf. orange lines in Fig. 2), in addition to the pure shifting of the pattern along the V_{D0} -axis. These lines arise because the charge center retains its configuration for the time-span determined by the tunneling time, even while its chemical potential crosses the charge transition point. To be specific, at I_B (cf. Fig. 2 (a)) no current is expected for the D^+ configuration, the equilibrium state at $V_P = 0$. When the additional voltage pulse is in the high state, the chemical potential is pushed over the charge transition point, into the region where D^0 is the equilibrium configuration. If an electron is captured (and D^0 is occupied) during this time, immediately after V_P is brought back to zero we will find the D^0 state at a gate configuration where a transport-line is present. Thus, $I_{SET} \neq 0$ when $V_P = 0$, until the electron tunnels out again. Observing a DC current in the orange shaded area around I_B indicates that the system is able to maintain a non-equilibrium state for a time comparable to the pulse duration, i.e. the tunnel rate

is comparable to the pulsing frequency f_P . Similar arguments hold for I_C and I_D , whereas the bias line around I_A is not altered, because the voltage pulse does not cause a charge transition of the center. Note that this symmetry break stems from the asymmetric pulsing between 0 V and V_P . The low-frequency limit is shown in Fig. 2 (b), where $f_P = 61.3$ Hz, and only a horizontally-shifted duplicate of the Coulomb peaks pattern is observed. In contrast, the data in Fig. 2 (c) illustrate the high-frequency limit $f_P = 5.12$ kHz, where we find $I_{\text{SET}} \neq 0$ at the location of non-equilibrium transport lines.

Quantitatively, the DC value of I_{SET} at the non-equilibrium current peaks can be understood within a rate equation model. When we pulse the chemical potential of the charge center over the charge transition level, the current state $D^{+/0}$ will either persist, because the stable state is reached, or change to the opposite state with the corresponding capture (Γ_c) or emission (Γ_e) rate. The probability to find at the point \downarrow in Fig. 2 (d) the D^+ state occupied is $P_{\downarrow}(D^+) = P_{\uparrow}(D^+)\exp(-\Gamma_c\tau_H)$, because during τ_H the system tends towards D^0 . Additionally, $P_{\downarrow}(D^0) = P_{\uparrow}(D^0) + P_{\uparrow}(D^+)(1 - \exp(-\Gamma_c\tau_H))$, because $P_{\downarrow}(D^0)$ is increased during τ_H . The same arguments hold for the inverse direction yielding $P_{\uparrow}(D^0) = P_{\downarrow}(D^0)\exp(-\Gamma_e\tau_L)$ and $P_{\uparrow}(D^+) = P_{\downarrow}(D^+) + P_{\downarrow}(D^0)(1 - \exp(-\Gamma_e\tau_L))$. To determine the four separate time durations, corresponding to occupation of either D^0 or D^+ , for both values of V_P , which we label $T_{L/H}(D^0/D^+)$ we express the probabilities $P_{\uparrow/\downarrow}(D^0/D^+)$ as a function of Γ_e and Γ_c . We integrate these probabilities, including the time evolution of the occupation of the charge state over the pulse length $\tau_{L/H}$, to obtain the average time, finding D^0/D^+ during $V_P = V_0/V_H$. The result is the four times of interest: $T_L(D^0) = (1/\Gamma_e)S$, $T_L(D^+) = \tau_L - (1/\Gamma_e)S$, $T_H(D^+) = (1/\Gamma_c)S$, and $T_H(D^0) = \tau_H - (1/\Gamma_c)S$, where $S = \frac{(1 - \exp(-\Gamma_c\tau_H))(1 - \exp(-\Gamma_e\tau_L))}{1 - \exp(-\Gamma_c\tau_H)\exp(-\Gamma_e\tau_L)}$.

The times obtained in this manner are proportional to I_{SET} . Since every transport-line has an individual current amplitude, we analyze the peak ratios $\frac{I_B}{I_A+I_B}$ and $\frac{I_D}{I_C+I_D}$ which are equal to the ratios $\frac{\tau_H}{\tau_H+T_L(D^0)}$ and $\frac{T_H(D^+)}{T_H(D^+)+T_L(D^+)}$, respectively. Although pulsing is performed parallel to the control gate axis, it is possible to compare current amplitudes from a cut along the top-gate axis, because the current amplitude does not vary significantly along specific transport-lines. Figure 3 (a) displays the peak ratios for a duty cycle of $d = 0.5$ as function of f_P . The ratios $\frac{I_B}{I_A+I_B}$ (black squares) and $\frac{I_D}{I_C+I_D}$ (green squares) are obtained from data like Fig. 2 (b) or (c) and both show a quantitative agreement with the model using $\Gamma_e = 1000 \text{ s}^{-1}$ and $\Gamma_c = 3000 \text{ s}^{-1}$ over the entire frequency range f_P . Fig. 3 (b) compares the model with the experimental data for a fixed $f_P = 61.3$ Hz as a function of the duty cycle d . Again, the

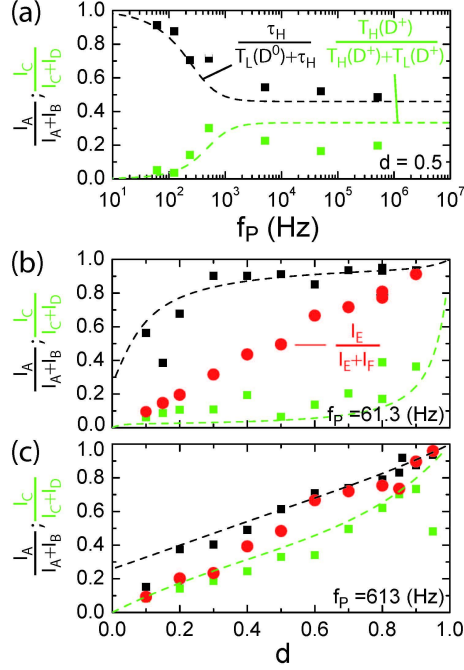


FIG. 3: Intensity ratios of the Coulomb peaks for points in the charge stability diagram (cf. Fig. 2 (a)) and time ratios originating from the rate equation model (dashed lines). Panel (a) shows the peak ratios as functions of the pulse frequency f_P for a duty cycle of 0.5. The dashed lines represent the model using a capture rate $\Gamma_c = 3000 \text{ s}^{-1}$ and an emission rate $\Gamma_e = 1000 \text{ s}^{-1}$. Panels (b) and (c) show the same ratios as function of the duty cycle for a fixed f_P of 61.3 Hz and 613 Hz, respectively, where experiment and model is in good agreement. Additionally, the red filled circles are the Coulomb peak ratios outside the region of the charge transition. They show good agreement with the ratios of τ_H and τ_L depending on the duty cycle d .

data is described well by the model using the same capture and emission rates. At $d \approx 0$ and $d \approx 1$, the peak ratios are more difficult to determine due to the low I_{SET} for one of the contributions, explaining the deviations from the model. For comparison, the duty cycle (red circles in Fig. 3 (b),(c)) is recovered from the spectra independently by analyzing the ratio $\frac{I_E}{I_E + I_F}$, showing good agreement with the duty cycle applied. Fig. 3 (c) shows the same plot as Fig. 3 (b) for a higher $f_P = 613 \text{ Hz}$, again in good agreement with the model.

An estimate of the distance between the charge center and the SET island can be obtained from the capacitive modeling of the charge transfer signal Δq , as shown in Ref. 12. For the specific geometry of the device measured here, we find that $\Delta q \sim 0.5e$ corresponds to a distance $\sim 40 \text{ nm}$. We use ISE-TCAD to calculate the profile of the conduction band

between donor and SET when the D^0 state is aligned with μ_{SET} , and from this, the area of the tunnel barrier. A WKB calculation of the tunnel rate yields $\Gamma \sim 10^4 \text{ s}^{-1}$, in reasonable agreement with experimental findings.

In summary, we demonstrated and analyzed the tunneling of electrons in a hybrid device consisting of ^{31}P donors implanted next to a gate-induced SiSET. We showed that the changes in the surrounding charge configuration can be sensitively detected by the SET, and the mutual coupling fulfills the requirements necessary for spin readout as proposed in Ref. [12]. We further demonstrated a technique to determine the tunnel rate of the center investigated, and this technique is applicable even when this tunnel rate exceeds the bandwidth of the detection SET. We also provide a quantitative tunnel rate model that agrees with the experimental findings. This experimental and theoretical toolbox paves the way to the use of spin-dependent electron tunneling as a readout method for single spins in silicon.

The authors thank D. Barber, N. Court, E. Gauja, R. P. Starrett, and K. Y. Tan for technical support at UNSW, and Alberto Cimmino for technical support at the Univ. of Melbourne. This work is supported by the Australian Research Council, the Australian Government, and by the U.S. National Security Agency (NSA) and U.S. Army Research Office (ARO) under Contract No. W911NF-08-1-0527. Work at Wisconsin was supported by ARO and LPS under Contract No. W911NF-08-1-0482.

-
- [1] B. E. Kane, *Nature* **393**, 133 (1998).
 - [2] V. Cerletti et al., *Nanotechnology* **16**, R27 (2005).
 - [3] J. M. Elzerman et al., *Nature* **430**, 431 (2004).
 - [4] C. Barthel et al., *Phys. Rev. Lett.* **103**, 160503 (2009).
 - [5] R. Hanson et al., *Rev. Mod. Phys.* **79**, 1217 (2007).
 - [6] J. Berezovsky et al., *Science* **314**, 1916 (2006).
 - [7] N. Shaji et al., *Nature Physics* **4**, 540 (2008).
 - [8] H. W. Liu et al., *Phys. Rev. B* **72**, 161305(R) (2005).
 - [9] M. Xiao et al., *Nature* **430**, 435 (2004).
 - [10] F. Jelezko et al., *Phys. Rev. Lett.* **92**, 076401 (2004).

- [11] H. Sellier et al., Phys. Rev. Lett. **97**, 206805 (2006).
- [12] A. Morello et al., Phys. Rev. B **80**, 081307(R) (2009).
- [13] D. N. Jamieson et al., Appl. Phys. Lett. **86**, 202101 (2005).
- [14] S. J. Angus et al., Nano Lett. **7**, 2051 (2007).
- [15] F. Hofmann et al., Phys. Rev. B **51**, 13872 (1995).
- [16] S. J. Angus et al., Appl. Phys. Lett. **92**, 112103 (2008).
- [17] B. C. Johnson et al., Thin Solid Films, doi:10.1016/j.tsf.2009.09.152 (2009).
- [18] W. H. Lim et al., Appl. Phys. Lett. **94**, 173502 (2009).
- [19] W. G. van der Wiel et al., Rev. Mod. Phys. **75**, 1 (2003).
- [20] L. Sun and B. E. Kane, Phys. Rev. B **80**, 153310 (2009).
- [21] G. P. Lansbergen et al., Nature Physics **4**, 656 (2008).
- [22] A. K. Ramdas and S. Rodriguez, Reports on Progress in Physics **44**, 1297 (1981).